Inorganic Chemistry

Article

pubs.acs.org/IC

Hybrid Inorganic–Organic Materials with an Optoelectronically Active Aromatic Cation: $(C_7H_7)_2SnI_6$ and $C_7H_7PbI_3$

Annalise E. Maughan, Joshua A. Kurzman, and James R. Neilson*

Department of Chemistry, Colorado State University, Fort Collins, Colorado 80523-1872, United States

Supporting Information

ABSTRACT: Inorganic materials with organic constituents—hybrid materials—have shown incredible promise as chemically tunable functional materials with interesting optical and electronic properties. Here, the preparation and structure are reported of two hybrid materials containing the optoelectronically active tropylium ion within tin- and lead-iodide inorganic frameworks with distinct topologies. The crystal structures of tropylium tin iodide, $(C_7H_7)_2SnI_6$, and tropylium lead iodide, $C_7H_7PbI_3$, were solved using high-resolution synchrotron powder X-ray diffraction informed by X-ray pair distribution function data and high-resolution time-of-flight neutron diffraction. Tropylium tin iodide contains isolated tin(IV)-iodide octahedra and crystallizes as a deep black solid, while tropylium lead iodide presents one-dimensional chains of face-sharing lead(II)-iodide octahedra and crystallizes as a bright red-orange powder. Experimental diffuse reflectance spectra are in good agreement with density functional calculations of the electronic structure. Calculations of the band decomposed charge densities suggest that the deep black color of tropylium tin iodide is attributed to iodide ligand to tin metal charge transfer, while the bright red-orange color of tropylium lead iodide arises from charge transfer between iodine and tropylium states. Understanding the origins of the observed optoelectronic properties of these two compounds, with respect to their distinct topologies and organic–inorganic interactions, provides insight into the design of tropylium-containing compounds for potential optical and electronic applications.

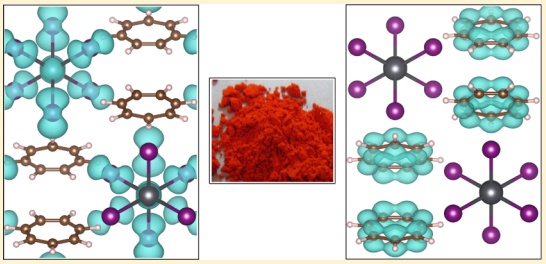

INTRODUCTION

Growing and novel technologies necessitate the discovery of new materials with robust and tunable properties. Hybrid materials—which in the present context we use to denote compounds composed of an inorganic lattice and primarily noncoordinating organic ions (i.e., not coordination polymers)—are an advantageous subset of functional materials that exhibit a wide range of optical and electronic properties.[1−3] Such materials are of particular interest for device applications because the properties and structures are easily tuned by chemical modification of either the inorganic or organic components.[1,4] Furthermore, the often solution-based synthetic routes used to prepare hybrid compounds enable facile production of films for device fabrication.[5,6] Specifically, main-group metal–halide-based hybrids are among the most widely researched, and often the observed properties derive primarily from the inorganic connectivity.[7] For example, lead and tin halide perovskites, including both purely inorganic (e.g., $CsSnI_3$ and $CsPbI_3$) and hybrid compounds (e.g., $CH_3NH_3SnI_3$ and $CH_3NH_3PbI_3$), show exceptionally high carrier mobilities and offer great promise in solar photoconversion applications;[8,9] replacement of the smaller Cs^+ cation with the larger methylammonium ($CH_3NH_3^+$) cation induces a lattice expansion and alteration of octahedral tilting that influences, among other characteristics, the band gap and mobility.[10,11] Similar effects can be achieved by replacing or substituting the smaller Br^- or Cl^- anions for the larger I^- anion, and collectively, these compositional variations can be exploited to enhance factors such as moisture stability,[12,13] a key factor in practical device longevity.

With significant research interest devoted to utilizing Pb–I and Sn–I frameworks as the inorganic component in functional hybrid materials, the size and functionality of the organic cation has been shown to greatly influence the dimensionality and connectivity of the inorganic lattice.[7,14] Small organic cations such as methylammonium and formamidinium result in three-dimensional hybrid perovskites,[1,9] while slightly larger primary cyclic ammonium cations like cyclobutylammonium form two-dimensional layered perovskites.[13,15] Larger cations often produce frameworks of reduced dimensionality; 1-D infinite chains of face- or edge-sharing octahedra are commonly observed.[16−18] Although lower dimensional compounds exhibit interesting photoluminescence properties, the structural connectivity typically inhibits carrier mobilities.[19] Additionally, zero-dimensional molecular compounds containing isolated polyhedra or small inorganic clusters tend to result when large organic ions or higher charged inorganic cations are present;[20] these compounds exhibit absorption features characteristic of the constituents rather than broad band spectral absorption.[21]

While the choice of organic cation can drastically affect the structure of the inorganic framework in hybrid materials, it does

Received: October 28, 2014
Published: December 19, 2014

 © 2014 American Chemical Society dx.doi.org/10.1021/ic5025795 | Inorg. Chem. 2015, 54, 370–378

not always influence the optoelectronic properties, owing to the fact that they are typically optoelectronically inactive in UV or visible light. Another approach to tune the properties of hybrid materials is to introduce an organic component with desirable optical and electronic properties. An exemplary molecule is the cycloheptatrienyl (tropylium) ion; tropylium is a seven-membered aromatic ring containing a delocalized positive charge and is a compelling choice for use in hybrid materials. Tropylium exhibits extraordinary charge transfer properties that are easily tuned by altering the polarity of the solvent environment.[22] Because of its aromaticity, the positive charge of tropylium is delocalized; therefore, the ion maintains its planar structure and is chemically stable as a reactant. This enables tropylium to be readily retained under a variety of synthetic conditions.[23,24] By introducing the tropylium ion into lead- and tin-iodide frameworks, the electronic properties may be enhanced through coupling of the inorganic lattice to the delocalized electron density in the tropylium ring.

Here, we report the preparation, crystal structures, and optoelectronic properties of tropylium tin iodide, $(C_7H_7)_2SnI_6$, and tropylium lead iodide, $C_7H_7PbI_3$, which are the first hybrid materials to incorporate the tropylium ion as the organic constituent. Tropylium tin iodide, $(C_7H_7)_2SnI_6$, is a black powder that crystallizes in space group *An* and contains isolated tin(IV)-iodide octahedra (Figure 1a and b); tropylium lead iodide, $C_7H_7PbI_3$, crystallizes as a bright red-orange powder in space group *Pnma* and contains one-dimensional lead(II)-iodide chains (Figure 1c and d). The crystal structures of these compounds were solved *ab initio* from high-resolution synchrotron X-ray powder diffraction data (SXRD), and high-resolution time-of-flight neutron diffraction was used to confirm the structure of tropylium tin iodide. The optical properties of tropylium tin iodide are commensurate with the molecular nature of the compound, evidenced by a large absorbance feature in the ultraviolet (UV) region consistent with intramolecular electronic transitions of the tropylium ion.

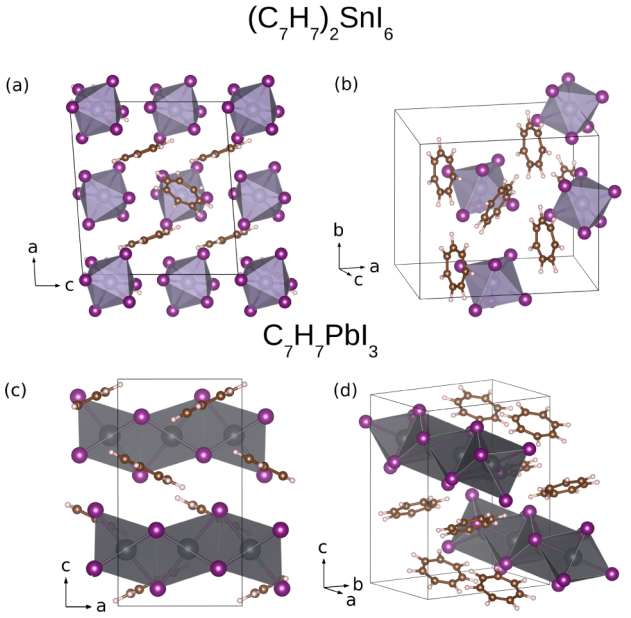

Figure 1. DFT-relaxed crystal structures of tropylium tin iodide (a, b) and tropylium lead iodide (c, d). Lavender spheres denote tin, purple denote iodine, charcoal denote lead, brown denote carbon, and eggshell denote hydrogen.

Electronic structure calculations indicate localized states consistent with the zero-dimensional inorganic components, well-separated tropylium cations, and extremely high measured electrical resistivity. The deep black color of $(C_7H_7)_2SnI_6$ and density functional theory (DFT) calculations suggest that charge transfer is not likely due to any inorganic–organic coupling but rather is solely due to the inorganic constituents. On the other hand, the bright red-orange color of tropylium lead iodide suggests increased charge transfer between the organic component and the inorganic lattice, evidenced by the fact that 1-D iodoplumbates typically range from colorless to yellow to orange.[16−18] DFT calculations of the band and *k*-point decomposed charge densities are used to probe the nature of optical transitions across the fundamental gaps, and support the presence of localized charge transfer to tropylium in $C_7H_7PbI_3$.

RESULTS AND DISCUSSION

Tropylium tin iodide was prepared by reaction of SnI_4 and tropylium iodide in aqueous hydroiodic acid, which resulted in a crystalline black product that rapidly precipitated out of the solution. As a control, preparation was attempted by reaction with tin(II) iodide; the final product was identical but contained a significant fraction of SnI_4, as supported by the facile oxidation of tin(II) to tin(IV).[25] Tropylium lead iodide was prepared by reaction of tropylium tetrafluoroborate and PbI_2 in aqueous hydroiodic acid, which resulted in a bright red-orange crystalline powder. There was no difference in the final product when tropylium iodide was synthesized first, followed by reaction with PbI_2.

FT-IR and ^{1}H NMR Studies. FT-IR spectra of compacted powders show the expected vibrational modes for the aromatic ring in all three tropylium containing compounds, C_7H_7I, $(C_7H_7)_2SnI_6$, and $C_7H_7PbI_3$ (Figure 2). The sharp peak at 3000 cm^{-1} indicates C—H stretching, while sharp signals at approximately 1460 and 1050 cm^{-1} identify C=C stretching and in-plane C—H bending, respectively. The feature at 650 cm^{-1} corresponds to an aromatic out-of-plane ("oop") C—H bend.[26,27]

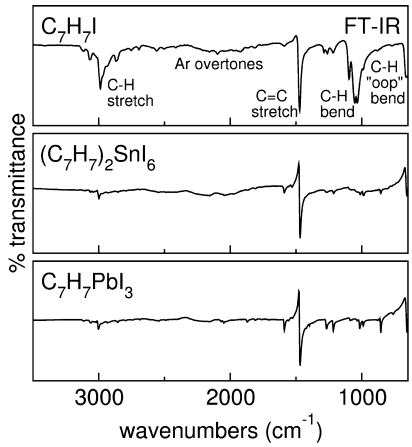

Figure 2. FT-IR spectra of tropylium iodide, tropylium tin iodide, and tropylium lead iodide, indicating the vibrational modes of the aromatic (Ar) $[C_7H_7]^+$ ring. "oop" refers to "out-of-plane" bending.

^{1}H and ^{19}F NMR spectroscopies were performed on solutions prepared from dissolving tropylium iodide, tropylium tin iodide, and tropylium lead iodide in d_6-DMSO. The proton

dx.doi.org/10.1021/ic5025795 | Inorg. Chem. 2015, 54, 370−378

spectra of all three compounds show a large singlet at a chemical shift of 9.33 ppm, which is consistent with the seven hydrogens of the aromatic tropylium ring (Figure 3). The small

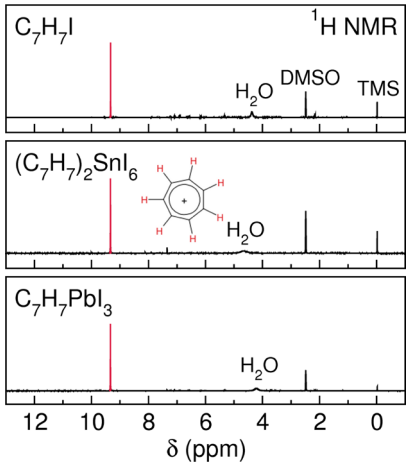

Figure 3. ^{1}H NMR spectra of tropylium iodide, tropylium tin iodide, and tropylium lead iodide redissolved in d_6-DMSO. The singlet at δ = 9.33 corresponds to the seven hydrogens of the aromatic tropylium ion, which are highlighted in red for clarity. Tetramethylsilane (TMS) was used as an internal standard.

peaks between 4 and 7 ppm in the ^{1}H NMR spectra indicate a benzaldehyde impurity, which may have formed from oxidation of the tropylium ion by hydroiodic acid. However, the concentration of this impurity is small compared to that of tropylium, was undetectable by other analytical methods, and does not appear to influence the structure of the lead and tin containing products. The ^{19}F NMR spectrum of tropylium iodide (not shown) reveals minor contributions from a tetrafluoroborate impurity, which is also confirmed by powder X-ray diffraction (14(6) mol %); however, there was no evidence for this impurity in the $(C_7H_7)_2SnI_6$ or $(C_7H_7)PbI_3$ products by ^{19}F NMR.

The Crystal Structures of Tropylium Tin Iodide, $(C_7H_7)_2SnI_6$, and Tropylium Lead Iodide, $C_7H_7PbI_3$. The crystal structures of tropylium tin iodide and tropylium lead iodide were solved *ab initio* from SXRD data. Unit cells were determined using DICVOL;[28] the large number of well-resolved reflections provided a lone plausible cell solution for each compound. Space group assignments were deduced by examining systematic absences in the data, as discussed in detail below. Inspection of X-ray pair distribution function (PDF) data enabled an *a priori* elucidation of tin and lead coordination environments. Sn−I pair correlations are observed at 2.9(2) Å, consistent with tetravalent SnI_6 octahedra rather than SnI_4 tetrahedra. Bond valence calculations for six-coordinate Sn with an average Sn−I bond distance of 2.9 Å are also consistent with the Sn^{4+} oxidation state.[29−31] (The bond valence parameters used for this calcultion (R_0 = 2.700(7), B = 0.37) were suggested by Hu et al.,[31] as determined from a survey of reported Sn(IV)−I crystal structures. We note that this parameter is not currently incorporated into the running list compiled by the International Union of Crystallography (http://www.iucr.org/resources/data/datasets/bond-valence-parameters, sourced 12/3/2014), which does not contain bond valence parameters for Sn(IV)−I. X-ray PDF data of tropylium lead iodide reveals a Pb−I pair correlation at 3.2(1) Å consistent with PbI_6 octahedra. The heavy atoms in both tropylium tin iodide and tropylium lead iodide were located utilizing the Monte Carlo algorithm implemented in FOX[32] by introducing rigid octahedral units with metal−ligand bond distances taken from the PDF data. Once the heavy atoms were located, electron density Fourier difference maps were generated from Rietveld refinements of the heavy atom positions against the SXRD data, which revealed rings of positive electron density consistent with the size of tropylium ions (Figure 4a and c). Carbon positions were

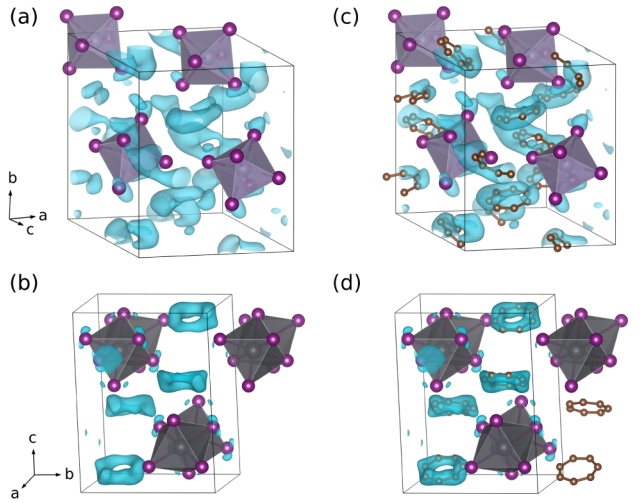

Figure 4. Visualization of the residual electron density after location of the heavy atoms in tropylium tin iodide (a) and tropylium lead iodide (b). Crystal structures of tropylium tin iodide (c) and tropylium lead iodide (d) are superposed on the respective Fourier difference maps. Hydrogen atoms have been omitted for clarity, lavender spheres denote tin atoms, charcoal are lead, purple are iodine, and brown are carbon.

located manually via maxima in the difference density, and also using rigid-body modeling (FOX) with frozen metal and iodide positions as determined from heavy-atom-only refinements. We elected to restrain the tropylium C−C bond distances to 1.35(5) Å and the internal angles of the ring to 128.6(1)° to encourage chemically rational representations of the aromatic ring,[33] the presence of which is confirmed by the FT-IR and ^{1}H NMR studies. Despite the success in locating carbon positions, the models most likely reflect the average positions of tropylium, which is liable to be rotationally disordered in both compounds.

Tropylium tin iodide, $(C_7H_7)_2SnI_6$, crystallizes in the monoclinic space group *An* with lattice parameters a = 14.5120(1) Å, b = 12.5472(1) Å, c = 13.0163(1) Å, and β = 94.303(1)°. Observed reflections in the SXRD data are consistent with space groups deriving from the *A*1*n*1 extinction symbol, namely, *An* and *A*2/*n*. Although the atomic positions can be described by significantly fewer symmetry distinct atoms in *A*2/*n*, the presence of inversion symmetry necessitates that one of the two troplyium ions in the asymmetric unit be described by split sites. A split-site (half-occupied) model to account for the carbon positions is not necessarily inappropriate, considering the expectation of rotational disorder, but such a model is challenging to restrain for refinement. Despite a larger number of free parameters, site-splitting is avoided with the use of space group *An*, which also provided for convenient generation of a fully occupied model as required for density functional calculations.

dx.doi.org/10.1021/ic5025795 | *Inorg. Chem.* 2015, 54, 370−378

In Figure 4b, the structure of $(C_7H_7)_2SnI_6$ is superposed on the Fourier difference map generated from a heavy-atom-only Rietveld refinement. A joint Rietveld refinement against the SXRD data and high-resolution time-of-flight neutron diffraction data was performed with all of the atoms in the unit cell, including hydrogen, and offers strong support of the *An* structural model determined using solely X-ray data (Figure 5). Although it was anticipated that incoherent scattering by

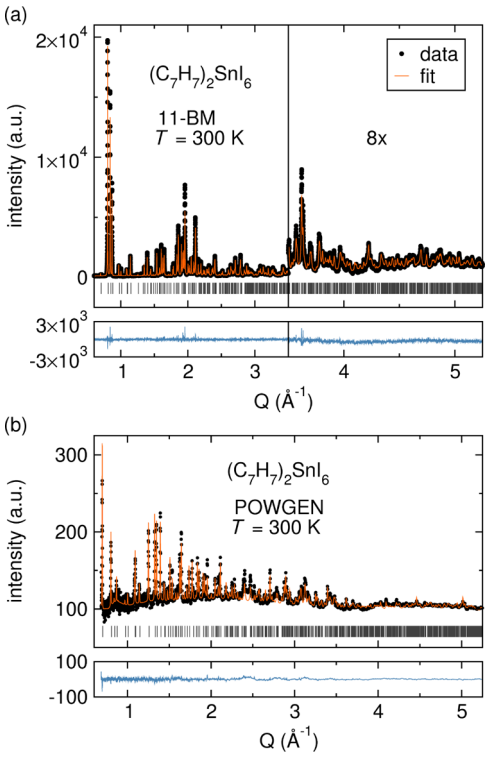

Figure 5. Joint Rietveld refinement of high-resolution X-ray powder diffraction data (a) with high-resolution time-of-flight neutron diffraction data (b). The right panel in part (a) is multiplied by 8 for ease of inspection. The gray tick marks indicate the locations of predicted Bragg reflections of $(C_7H_7)_2SnI_6$. Refinement parameters can be found in Table 1.

hydrogen might dominate the pattern, the data present well-resolved reflections (Figure 5b). In addition to C−C bond distance and angle restraints, the inclusion of hydrogen necessitated C−H distance [1.10(5) Å] and C−C−H angle [115.7(1)°] restraints to preserve the planarity of the tropylium ion. While the smeared electron density present in Figure 4a and b is suggestive of rotational disorder of tropylium, the refined atomic displacement parameter (ADP, U_{iso}, Table 1) on carbon is consistent with a lesser degree of disorder than expected; this lends support to the choice of space group *An* rather than *A*2/*n* to model the compound. The X-ray refinement shown in Figure 5a exhibits diffuse features at higher *Q*, and despite the exceptional flux and signal-to-noise provided by the 11-BM diffractometer, there were no observable Bragg features beyond $Q = 6$ Å^{-1}. These observations indicate orientational disorder of the isolated SnI_6 octahedra, which is a common consequence of isolated octahedral units (cf., SF_6[34] and K_3AlF_6).[35] This is also reflected in the large heavy-atom U_{iso} values obtained from the refinement.

Table 1. Structural Parameters and Refinement Statistics for Tropylium Tin Iodide and Tropylium Lead Iodide[a]

	$(C_7H_7)_2SnI_6$	$C_7H_7PbI_3$
crystal system	monoclinic	orthorhombic
space group	*An*	*Pnma*
a (Å)	14.5120(1)	8.05443(2)
b (Å)	12.5472(1)	11.18714(3)
c (Å)	13.0163(1)	14.71927(5)
α (deg)	90	90
β (deg)	94.303(1)	90
γ (deg)	90	90
U_{iso}(M) (Å^2)	0.051(1)	0.0461(2)
U_{iso}(I) (Å^2)	0.0422(2)	0.0685(5); 8*d* 0.0640(6); 4*c*
U_{iso}(C) (Å^2)	0.0164(6)	0.102(4)
U_{iso}(H) (Å^2)	0.064(3)	
red. χ^2	4.8	3.31
wR_p	4.7%	10.2%

[a]With the exception of the two chemically distinct iodine atoms in $C_7H_7PbI_3$ (indicated by Wyckoff sites), like elements were constrained to the same atomic displacement parameter. Refinement statistics for $(C_7H_7)_2SnI_6$ are reported for the joint X-ray and neutron refinement.

Tropylium lead iodide, $C_7H_7PbI_3$, crystallizes in the orthorhombic space group *Pnma* with lattice parameters $a = 8.05443(2)$ Å, $b = 11.18714(3)$ Å, and $c = 14.71927(5)$ Å. On the basis of the observed extinctions (extinction symbol *P*−*cn*), two possible space groups were identified, $P2_1cn$ and *Pmcn*; the conventional settings, $Pna2_1$ and *Pnma*, were adopted for structure determination and refinement. Analogous topologies containing one-dimensional chains of face-sharing PbI_6 octahedra were found for both space group possibilities. In $Pna2_1$, for which the 4*a* general position is the only Wyckoff position, three unique iodines are required in the asymmetric unit. In space group *Pnma*, the same topology is described by one Pb and two I atoms, with one of the crystallographically distinct iodine atoms residing on the 8*d* general position. The larger number of atoms required in $Pna2_1$ and lack of statistical improvement despite the increase in free parameters support the selection of *Pnma*.[36] Tropylium ions are described by four crystallographically distinct carbon atoms, one of which resides on a mirror plane normal to *b* (the 4*c* position). In Figure 4d, the resulting structural model is superposed on the difference map generated from the carbon-free model.

As similarly noted for the tin compound, the diffraction pattern of $C_7H_7PbI_3$ presents diffuse components in the higher *Q* region (Figure 6), and there are no observable Bragg features beyond $Q = 7$ Å^{-1}. This indicates that Pb and I are also somewhat disordered in tropylium lead iodide, as reflected by the ADPs (Table 1). While large ADPs could be an indication of an error in space group selection, we note that slighly larger U_{iso} values were obtained in refinements using space group $Pna2_1$, which further supports the space group selection and the notion of intrinsic structural disorder. The $Pna2_1$ and *Pnma* structures differ with respect to the tropylium orientation, which is slightly canted in the *bc* plane in $Pna2_1$. Density functional relaxation in both space groups, constrained to the experimentally determined cell, suggests a slight stabilization of 35 meV per formula unit in $Pna2_1$. However, as discussed in more detail below, since this is not the DFT equilibrium cell volume, it is difficult to be certain which structure is more energetically favorable. Despite identical Rietveld refinement

dx.doi.org/10.1021/ic5025795 | *Inorg. Chem.* 2015, 54, 370−378

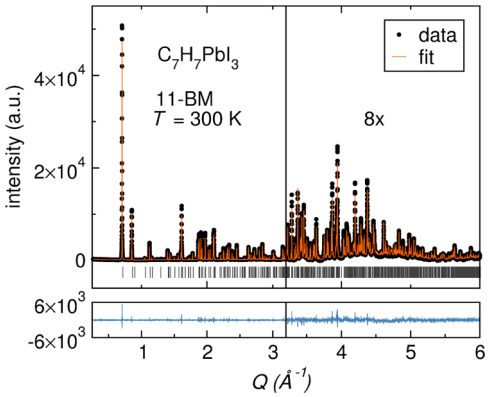

Figure 6. Rietveld refinement of tropylium lead iodide. The data for $Q > 3.2$ Å^{-1} are multiplied by 8 in order to enhance the diffuse features at higher Q. The gray tick marks indicate the locations of predicted Bragg reflections for $C_7H_7PbI_3$.

statistics, the fewer number of structural parameters required to describe $C_7H_7PbI_3$ in *Pnma* is consistent with the room temperature structure adopting this space group.

Further refinement of the $(C_7H_7)_2SnI_6$ and $C_7H_7PbI_3$ models against X-ray PDF data indicates that the local structures are described well by the average structures, as shown in parts a and b of Figure 7, respectively. Medium-range structural disorder, however, is reflected in the poorly predicted intensities of intraoctahedon features in full-range refinements: in tropylium tin iodide, the Sn–I (r = 2.9(2) Å) and *cis*-I–I (r = 4.1(2) Å) intensities are poorly fit; in tropylium lead iodide, the *trans*-iodide feature at r = 6.4 Å (denoted by an arrow in Figure 7b) is poorly fit. The hypothesis of *inter*-octahedral disorder in both compounds is confirmed by refining the data over shorter correlation distances to minimize the effects of reduced coherence at longer length scales. As shown in the insets of Figure 7a and b, the predicted intensities of these low r features are notably improved by excluding longer r correlations. This strongly supports our assertions that the large ADPs obtained in Rietveld refinements arise from medium-range disorder, rather than due to problems inherent to the models. In $C_7H_7PbI_3$, the disorder is attributed to torsional distortions of the one-dimensional Pb–I chains.

OPTICAL PROPERTIES AND ELECTRONIC STRUCTURES

UV–Visible Diffuse Reflectance Spectroscopy. The Kubelka–Munk transform was performed on UV–visible diffuse reflectance spectra collected on powders of tropylium iodide, tropylium tin iodide, and tropylium lead iodide, and Tauc plots were generated to highlight possible direct and indirect absorption edges, as shown in Figure 8a and b, respectively. When the spectra are plotted as $[h\nu F(R)]^2$ (panel a), both tropylium iodide and tropylium tin iodide do not exhibit a well-defined direct optical band edge within the examined energy range. However, there is a strong absorption feature between 5 and 6 eV that corresponds to UV absorption by the tropylium ring, indicating that the electronic states of the tropylium ion are not strongly influenced by the surrounding inorganic constituents in $(C_7H_7)_2SnI_6$; this feature reflects the molecular nature of tropylium iodide and tropylium tin iodide. In contrast, tropylium lead iodide clearly shows a linear region in the Tauc plot that indicates a direct optical band gap of 2.15(1) eV when extrapolated to zero absorption. Additionally,

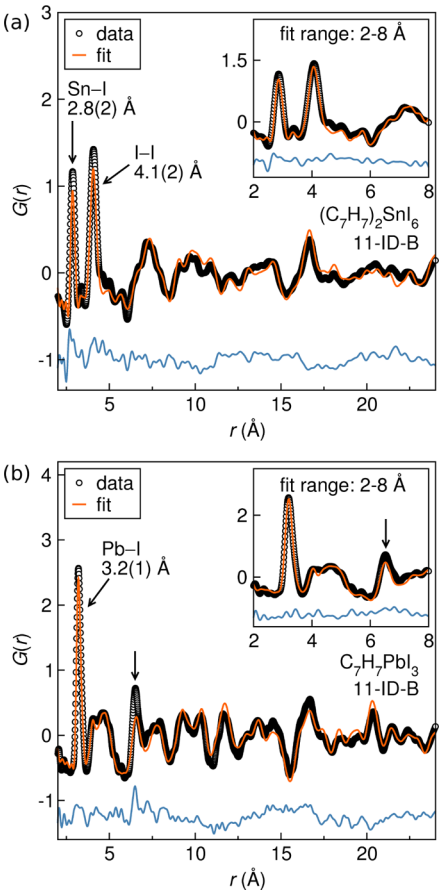

Figure 7. X-ray PDF analysis of (a) tropylium tin iodide and (b) tropylium lead iodide over a fit range of 2 Å < r < 24 Å. The insets of parts a and b show the refinements resulting from a fit range of 2 Å < r < 8.5 Å and 2 Å < r < 8 Å, respectively. The large feature in part a at r = 2.83 Å corresponds to the octahedral tin–iodide bond distance, while the peak at r = 4.44 Å reflects the distance between iodine atoms within an octahedron. In part b, the arrows show that, over shorter refinement ranges, the predicted intensity of the feature at $r \sim 6.4$ Å is improved.

the strong absorption feature characteristic of the $[C_7H_7]^+$ moeity is not resolved, which could be attributed to increased inorganic–organic interaction in the form of charge transfer.

When the diffuse reflectance data are plotted as $[h\nu F(R)]^{1/2}$ to highlight potential indirect band edges (Figure 8b), linear regions for tropylium iodide, tropylium tin iodide, and tropylium lead iodide are visible; extrapolation to zero absorption results in indirect gaps of 1.82(2), 1.20(6), and 1.97(1) eV, respectively. Although the Tauc plots of all three compounds exhibit broad absorption features across the range of energies examined, the absorption feature characteristic of the tropylium rings is still visible in the spectra of tropylium iodide and tropylium tin iodide, which supports the notion that there is minimal electronic coupling to the organic. In the absorption spectrum of tropylium lead iodide, the absorption peak of the tropylium ring is not resolved, which once again suggests that it may be obscured by inorganic–organic charge transfer.

We attribute the deep colors of tropylium tin iodide and tropylium lead iodide to charge-transfer processes, although the origin of these processes is not immediately apparent upon inspection of the optical spectra. In tropylium tin iodide, the charge-transfer processes are not likely due to any interaction

dx.doi.org/10.1021/ic5025795 | Inorg. Chem. 2015, 54, 370–378

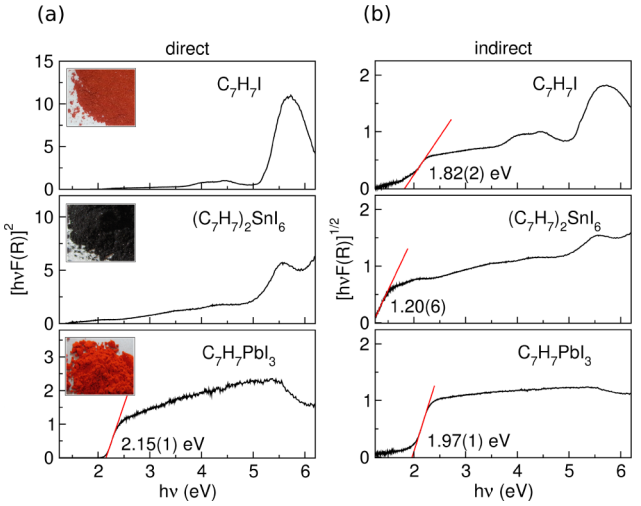

Figure 8. Tauc plots of UV−visible diffuse reflectance spectra used to determine the (a) direct optical gaps and (b) indirect optical gaps of tropylium iodide, tropylium tin iodide, and tropylium lead iodide (diluted in $BaSO_4$). The insets in part a are brightfield photographs of the sample powders of tropylium iodide, tropylium tin iodide, and tropylium lead iodide.

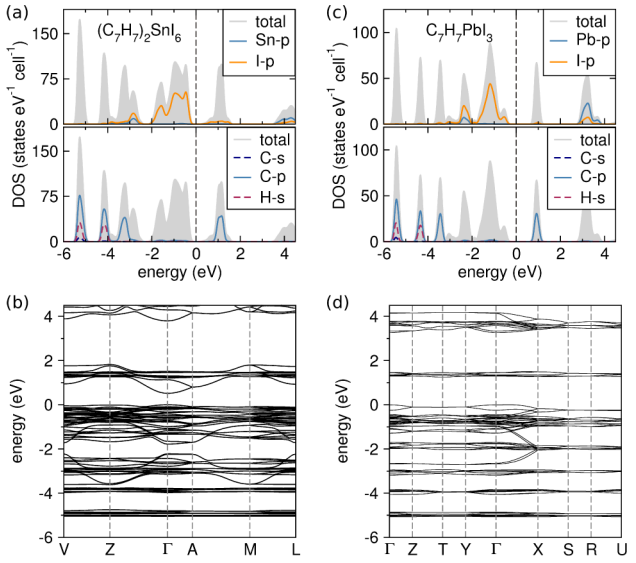

Figure 9. Total and local density of states for tropylium tin iodide (a) and tropylium lead iodide (c). The contributions from the inorganic constituents are shown in the upper panels, while the contributions from the tropylium rings are shown in the lower panels. The calculated band diagrams for tropylium tin iodide and tropylium lead iodide are shown in parts b and d, respectively. The Fermi energy is referenced to the top of the valence band, set to 0 eV.

between the tropylium cations and the isolated SnI_6 octahedra, due to the fact that the absorption feature of tropylium is highly pronounced. Therefore, it is much more likely that ligand-to-metal charge transfer is occurring between iodine and tin, thus resulting in the deep black color. In the case of tropylium lead iodide, it is interesting to compare the color of this compound to the colors of compounds with similar topologies. Typically, hybrid materials containing one-dimensional chains of face-sharing lead-iodide octahedra are reported to range in color from colorless to yellow-orange, regardless of the choice of organic constituent.[16,37,38] The anomalous bright red-orange color of the tropylium lead iodide powder suggests that there is strong charge transfer between the tropylium ions and the inorganic lattice, thus resulting in the unresolved absorption feature of tropylium in the absorbance spectrum of tropylium lead iodide.

DFT Calculations. The structures of tropylium tin iodide and tropylium lead iodide were optimized within density functional theory, and the relaxed structures were used in static electronic structure calculations. Due to the slow convergence of forces on tropylium rings when the lattice shape (i.e., cell dimensions) was allowed to relax at a fixed volume, ionic relaxations were constrained to the experimentally determined cells with respect to both volume and shape. Thus, the calculations presented here do not represent the electronic structures at equilibrium cell volumes, which may influence the magnitude of the calculated gaps. The DFT relaxed structures are in excellent agreement with the experimentally determined structures.

Total and local densities of states (DOS) and band structure diagrams are shown for both compounds in Figure 9. Tropylium tin iodide (panels a and b) is predicted to have a direct gap of 0.52 eV at the Γ point, which is consistent with the black color of the solid. The indirect gap between Γ and A is calculated to be 0.80 eV. Near the Fermi energy, the valence band is composed of primarily iodine *p* states, while the low-lying unoccupied states are predominantly iodine and, at slightly higher energies, carbon *p* states (panel a). The majority of bands present flat dispersions, with a few exceptions arising from a short I−I distance in the crystal structure. Orientational disorder of SnI_6 octahedra would relieve this contact and induce a narrowing of the dispersions, and the electronic states are probably more localized than reflected here. The generally localized states are consistent with tropylium tin iodide comprising isolated SnI_6 octahedra and tropylium ions, and this is reflected in a very high measured electrical resistivity. In this light, it is interesting to note that Cs_2SnI_6, a zero-dimensional "perovskite" containing regular isolated $[SnI_6]^{2-}$ units, exhibits high electron and hole mobility due to wider band dispersions that arise from increased overlap of iodine and tin states.[39]

The calculated DOS and band structure of tropylium lead iodide are shown in Figure 9c and d. An indirect gap of 1.25 eV is predicted to occur between roughly the Γ and T points; the highest occupied state actually occurs between Γ and X. The 1.3 eV direct gap at Γ is only slightly larger. In general, $C_7H_7PbI_3$ presents some similar electronic structural features as $(C_7H_7)_2SnI_6$, with localized carbon states suggesting minimal coupling between tropylium rings and metal/halide states. In contrast to tropylium tin iodide, however, the DOS indicate that the lowest-lying unoccupied states in $C_7H_7PbI_3$ have significant carbon character. Occupied iodine *p* states between −2.5 and 0 eV are somewhat disperse due to orbital overlap within the 1D chains.

Although the DFT calculations suggest that neither compound presents features expected to yield mobile charge carriers, supported by experimentally measured electrical resistivities in excess of $\sim 3 \times 10^7$ Ω cm, the DOS and band structures are reflective of the observed optical absorption behavior. To gauge the character of band-edge optical transitions, band and *k*-point decomposed charge densities were calculated at the valence band maxima (HOB, highest occupied band) and conduction band minima (LUB, lowest unoccupied band), presented in Figure 10. The HOB of $(C_7H_7)_2SnI_6$ (panel a) is composed of localized iodine *p* states

dx.doi.org/10.1021/ic5025795 | *Inorg. Chem.* 2015, 54, 370−378

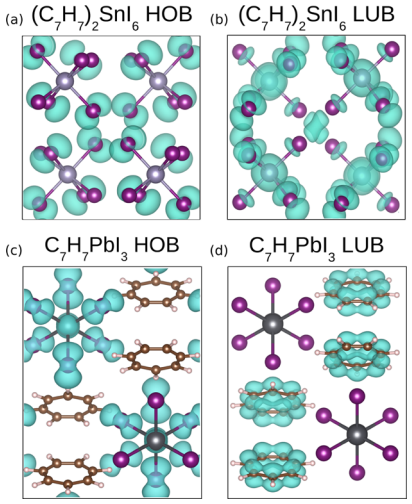

Figure 10. Band decomposed charge densities for tropylium tin iodide and tropylium lead iodide. Panel a shows the charge density associated with the highest occupied band (HOB) of tropylium tin iodide, while panel b shows the charge density of the tropylium tin iodide lowest unoccupied band (LUB). The band decomposed charge densities of tropylium lead iodide are shown in parts c and d, where part c illustrates the charge density of the HOB and part d shows the charge density for the LUB. The tropylium rings have been omitted from panels a and b for clarity.

while the LUB (panel b) contains significant Sn character, suggesting that near-edge optical absorption arises from ligand-to-metal charge transfer in tropylium tin iodide. The situation is distinct in $C_7H_7PbI_3$, in which charge density is localized on I and Pb at the HOB (panel c) but is almost entirely tropylium derived (π^* character) at the LUB (panel d). This scenario is highly suggestive of iodine-to-tropylium charge transfer, indicating stronger inorganic−organic interactions in the lead compound than in the tin.

CONCLUSIONS

We have prepared two hybrid materials containing the tropylium ion, an optoelectronically active unfunctionalized aromatic organic ion. The crystal structures of tropylium tin iodide, $(C_7H_7)_2SnI_6$, and tropylium lead iodide, $C_7H_7PbI_3$, were solved using high-resolution synchrotron powder X-ray diffraction informed by X-ray pair distribution function data. High-resolution time-of-flight neutron diffraction confirms the tropylium tin iodide structural model, which contains isolated $Sn^{IV}I_6$ octahedra. Tropylium lead iodine presents 1D chains of face-sharing $Pb^{II}I_6$ octahedra. The low dimensionality of both compounds contributes to high measured electrical resistivities, in excess of $\sim 3 \times 10^7$ Ω cm. The diffuse reflectance spectrum of tropylium tin iodide reveals a large absorption feature characteristic of the tropylium ion, suggesting that the optoelectronic properties result from intramolecular transitions of the SnI_6 octahedra and tropylium ion. Tropylium lead iodine, on the other hand, exhibits a broad spectral absorption, suggestive of increased electronic coupling between tropylium ions and the inorganic lattice. These conclusions are supported by density functional calculations of the band and *k*-point decomposed charge densities at the highest occupied and lowest unoccupied bands. The larger degree of organic−inorganic coupling observed for tropylium lead iodide motivates a search for tropylium-containing compounds with higher inorganic dimensionality, which may further increase the electronic coupling while also enabling improved carrier mobility.

EXPERIMENTAL SECTION

Materials. HI (57% aq., 1.5% H_3PO_2) was purchased from Sigma-Aldrich (99.99%), tropylium tetrafluoroborate from Alfa Aesar (99.99%) and kept in an argon inert atmosphere until use, tin metal shot (reagent grade) from Alfa Aesar, and iodine (99.8%) from Macron Chemicals. All chemicals were used without further purification.

Preparation of Tin(IV) Iodide (SnI_4). Tin metal (0.3108 g, 2.62 mmol) and iodine (1.3347 g, 5.26 mmol) were reacted in an evacuated fused silica ampule (P < 10 mTorr). The ampule was heated in a furnace at 200 °C for 48 h, which was air-quenched to yield bright orange-yellow SnI_4.

Preparation of Tropylium Iodide (C_7H_7I). At 60 °C, finely ground tropylium tetrafluoroborate (0.5177 g, 2.91 mmol) was added to 60 mL of ethanol in a 250 mL round-bottom flask with an air condenser; this solution was stirred vigorously to dissolve into a light yellow-brown solution. After boiling the ethanol for 5 min, the flask was removed from heat. When the rolling boil had subsided to a very gentle boil, 500 μL of stabilized HI solution (57% aq., 1.5% H_3PO_2) was added. This turned the solution dark red. After about 1 min of stirring, a bright red precipitate formed. The solution was stoppered and allowed to stir gently until cool. The flask was then submerged in an ice bath and stirred gently for 1 h. The solution and the precipitate were washed with anhydrous ether and centrifuged, which was repeated three times. The bright red precipitate was dried in an oven at 37 °C for 24 h, yielding a fine red powder of tropylium iodide (C_7H_7I, $R\bar{3}m$) with a small tropylium tetrafluoroborate impurity.[40]

Preparation of Tropylium Tin Iodide ($(C_7H_7)_2SnI_6$). A 100 mL two-necked round-bottom flask was charged with 7.0 mL of stabilized HI (57% aq., 1.5% H_3PO_2). The mixture was degassed with nitrogen for 1 min, and the flask was kept under nitrogen for the duration of the experiment. The flask was heated in an oil bath to 100 °C, and tin(IV) iodide (0.1834 g, 0.292 mmol) was added and then stirred vigorously until the solid had dissolved completely. Tropylium iodide (0.1279 g, 0.586 mmol) was then added to the flask, which immediately resulted in a black precipitate. The solution was stirred for an additional 15 min, at which time the heat was removed and the flask was allowed to air-cool while stirring gently. The solution and precipitate were washed with anhydrous ether and centrifuged three times. The black product was dried at 37 °C for 24 h. Compositional analysis confirms C 12.77%, H 1.11%, Sn 14.3%, and I 73.08% (Predicted: C 15.83%, H 1.33%, Sn 11.17%, I 71.67%).

Preparation of Tropylium Lead Iodide ($C_7H_7PbI_3$). A 100 mL two-necked round-bottom flask was charged with 11.0 mL of HI (57% aq., 1.5% H_3PO_2) and a stir bar. The solution was degassed with nitrogen for 1 min, and the flask was kept under nitrogen for the duration of the experiment. The flask was heated in an oil bath to 45 °C while stirring, at which point lead iodide (0.6438 g, 1.395 mmol) was added all at once and stirred vigorously to dissolve, resulting in a translucent bright yellow solution. The flask was heated to 55 °C at which point finely ground tropylium tetrafluoroborate (0.2483 g, 1.396 mmol) was added, turning the solution bright orange-red. The heat was immediately turned off, and the flask was allowed to cool in the warm oil bath while stirring gently. Once the temperature of the oil bath decreased to 40 °C, the flask was removed and allowed to air-cool to room temperature while stirring gently. Once cool, the solution and red precipitate were washed with ethanol and centrifuged. The remaining product was then washed with anhydrous ether and centrifuged three times. The resulting bright red precipitate was dried at 37 °C for 24 h. Compositional analysis confirms C 12.25%, H 1.07%, Pb 31.2%, and I 55.23% (Predicted: C 12.38%, H 1.04%, Pb 30.52%, I 56.06%).

Characterization. Products were characterized by high-resolution synchrotron powder X-ray diffraction data obtained from the diffractometer on beamline 11-BM-B at the Advanced Photon Source, Argonne National Laboratory.[41] Room temperature powder neutron

dx.doi.org/10.1021/ic5025795 | *Inorg. Chem.* 2015, 54, 370−378

diffraction data were collected on a sample sealed in a vanadium canister at the Spallation Neutron Source (SNS) at the Oak Ridge National Laboratory using the POWGEN diffractometer (BL-11A). After determination of the lattice parameters with DICVOL[28] and deduction of the space group from systematic absences, structural models were constructed using Free Objects for Crystallography (FOX).[32] The data were analyzed with the Rietveld method using GSAS/EXPGUI.[42] In order to generate the CIF files provided in the Supporting Information, the carbon−carbon bond distances were restrained to 1.35(5) Å and the bond angles were restrained to 128.6(1)° to create an idealized structural representation of the tropylium rings within the inorganic framework. X-ray scattering data suitable for pair distribution function (PDF) analysis were collected at beamline 11-ID-B at the Advanced Photon Source, Argonne National Laboratory, using 58 keV photons and a sample−detector distance of ∼17 cm. Experimental PDFs were extracted using PDFgetX3[43] and analyzed using PDFgui.[44] VESTA was used to visualize and render all crystal structures presented in this manuscript.[45]

Proton and fluorine nuclear magnetic resonance studies were performed on an Agilent (Varian) 400 MHz NMR spectrometer in deuterated d_6-DMSO. Fourier transform infrared spectroscopy (FT-IR) was performed on solid samples on a Thermo Nicolet iS50 FT-IR spectrometer from 650 to 4000 cm^{-1}. UV−visible diffuse reflectance spectroscopy was performed on powdered samples of all three tropylium compounds diluted to 15 wt % in $BaSO_4$, using $BaSO_4$ as a baseline; spectra were acquired using a Thermo Nicolet Evolution 300 spectrophotometer with a Praying Mantis mirror setup from λ = 200 to 1000 nm at a scan rate of 240 nm/min. Compositional analyses were performed at Galbraith Laboratories. Electronic resistance measurements on pellets with Au−paste contacts and Pt wires were attempted using a Physical Properties Measurement System (Quantum Design, Inc.); however, the resistivity exceeded that of the sensitivity of the instrument.

DFT Calculations. The electronic structures of $(C_7H_7)_2SnI_6$ and $C_7H_7PbI_3$ were calculated using density functional theory within the plane-wave code VASP (Vienna Ab initio Simulation Package).[46,47] The Perdew−Burke−Ernzerhof (PBE) functional[48] was used to treat the effects of exchange correlation at the generalized gradient approximation (GGA) level of theory. Valence−core interaction was described with the projector augmented wave method, and cores of $[Kr]4d^{10}$ for Sn and I, $[Xe]4f^{14}5d^{10}$ for Pb, and [He] for C were used. The structures of both compounds were relaxed within the constraints of the experimentally determined cells; attempts to determine the equilibrium structures by relaxing at a series of volumes were impeded by difficulty converging forces on the tropylium ring when the cell shape was allowed to change (for a fixed volume). Relaxations of the ionic positions were conducted using 2 × 6 × 4 for $(C_7H_7)_2SnI_6$ and 6 × 4 × 2 for $(C_7H_7PbI_3)$ Γ-centered k-point meshes and an energy cutoff of 520 eV. Relaxations were deemed to have converged when forces on all the ions were less than 0.02 eV $Å^{-1}$. The density of states of tropylium tin iodide was calculated using a 4 × 8 × 6 Γ-centered k-mesh with a total of 70 irreducible k points, and the band structure was calculated using 20 point interpolations along high symmetry directions of the first Brillouin zone (100 irreducible k points). The density of states of tropylium lead iodide was calculated using a 10 × 8 × 6 gamma-centered k-point mesh and the band structure was calculated using 15 point interpolations, both involving 120 irreducible k points.

■ ASSOCIATED CONTENT

Supporting Information

Crystallographic Information Files (CIFs), including atomic coordinates and atomic displacement parameters, of the title compounds. Also included are CIFs of the DFT-relaxed structures of the title compounds. This material is available free of charge via the Internet at http://pubs.acs.org.

■ AUTHOR INFORMATION

Corresponding Author

*E-mail: james.neilson@colostate.edu.

Notes

The authors declare no competing financial interest.

■ ACKNOWLEDGMENTS

The authors thank Prof. M. M. Reynolds for the use of her optical spectrometer and the expert staff of the Central Instrumentation Facility at Colorado State University for assistance with the FTIR and NMR characterization. The authors also thank the expert instrument scientists at 11-BM, O. Borkiewicz, and A. Huq for synchrotron X-ray and neutron data acquisition. The research reported in this publication was supported by the Energy Institute at Colorado State University. Use of the Advanced Photon Source at Argonne National Laboratory was supported by the U.S. Department of Energy, Office of Science, Office of Basic Energy Sciences, under Contract No. DE-AC02-06CH11357. This research utilized the CSU ISTeC Cray HPC System supported by NSF Grant CNS-0923386. A portion of this research at ORNL's Spallation Neutron Source was sponsored by the Scientific User Facilities Division, Office of Basic Energy Sciences, U.S. Department of Energy.

■ REFERENCES

(1) Mitzi, D.; Feild, C.; Schlesinger, Z.; Laibowitz, R. *J. Solid State Chem.* **1995**, *114*, 159−163.
(2) Mitzi, D. B.; Chondroudis, K.; Kagan, C. R. *IBM J. Res. Dev.* **2001**, *45*, 29−45.
(3) Tan, Z.-K.; Moghaddam, R. S.; Lai, M. L.; Docampo, P.; Higler, R.; Deschler, F.; Price, M.; Sadhanala, A.; Pazos, L. M.; Credgington, D.; Hanusch, F.; Bein, T.; Snaith, H. J.; Friend, R. H. *Nat. Nanotechnol.* **2014**, *9*, 687−692.
(4) Cheetham, A. K.; Rao, C.; Feller, R. K. *Chem. Commun.* **2006**, *46*, 4780−4795.
(5) Mitzi, D. B. *J. Mater. Chem.* **2004**, *14*, 2355−2365.
(6) Sun, S.; Salim, T.; Mathews, N.; Duchamp, M.; Boothroyd, C.; Xing, G.; Sum, T. C.; Lam, Y. M. *Energy Environ. Sci.* **2014**, *7*, 399−407.
(7) Knutson, J. L.; Martin, J. D.; Mitzi, D. B. *Inorg. Chem.* **2005**, *44*, 4699−4705.
(8) Mitzi, D.; Wang, S.; Feild, C.; Chess, C.; Guloy, A. *Science* **1995**, *267*, 1473−1476.
(9) Stoumpos, C. C.; Malliakas, C. D.; Kanatzidis, M. G. *Inorg. Chem.* **2013**, *52*, 9019−9038.
(10) Hao, F.; Stoumpos, C. C.; Chang, R. P.; Kanatzidis, M. G. *J. Am. Chem. Soc.* **2014**, *136*, 8094−8099.
(11) Borriello, I.; Cantele, G.; Ninno, D. *Phys. Rev. B* **2008**, *77*, 235214.
(12) Noh, J. H.; Im, S. H.; Heo, J. H.; Mandal, T. N.; Seok, S. I. *Nano Lett.* **2013**, *13*, 1764−1769.
(13) Billing, D. G.; Lemmerer, A. *CrystEngComm* **2006**, *8*, 686−695.
(14) Mercier, N.; Louvain, N.; Bi, W. *CrystEngComm* **2009**, *11*, 720−734.
(15) Billing, D. G.; Lemmerer, A. *CrystEngComm* **2007**, *9*, 236−244.
(16) Duan, H.-B.; Zhao, H.-R.; Ren, X.-M.; Zhou, H.; Tian, Z.-F.; Jin, W.-Q. *Dalton Trans.* **2011**, *40*, 1672−1683.
(17) Zhao, S.-P.; Ren, X.-M. *Dalton Trans.* **2011**, *40*, 8261−8272.
(18) Wang, G.-E.; Jiang, X.-M.; Zhang, M.-J.; Chen, H.-F.; Liu, B.-W.; Wang, M.-S.; Guo, G.-C. *CrystEngComm* **2013**, *15*, 10399−10404.
(19) Umebayashi, T.; Asai, K.; Kondo, T.; Nakao, A. *Phys. Rev. B* **2003**, *67*, 155405.
(20) Vincent, B. R.; Robertson, K. N.; Cameron, T. S.; Knop, O. *Can. J. Chem.* **1987**, *65*, 1042−1046.

(21) Pradeesh, K.; Agarwal, M.; Rao, K. K.; Prakash, G. V. *Solid State Sci.* **2010**, *12*, 95−98.
(22) Kosower, E. M. *J. Org. Chem.* **1964**, *29*, 956−957.
(23) Doering, W.; Knox, L. *J. Am. Chem. Soc.* **1957**, *79*, 352−356.
(24) Harmon, K. M.; Harmon, A. B.; Alderman, S. D.; Gebauer, P. A.; Hesse, L. L. *J. Org. Chem.* **1967**, *32*, 2012−2013.
(25) Cotton, F. A.; Wilkinson, G.; Murillo, C. A.; Bochmann, M.; Grimes, R. *Advanced Inorganic Chemistry*; Wiley: New York, 1999; Vol. 5.
(26) Sourisseau, C. *Spectrochim. Acta, Part A* **1978**, *34*, 881−887.
(27) Stuart, B. *Infrared Spectroscopy: Fundamentals and Applications*; John Wiley & Sons, Ltd.: Chichester, West Sussex, England, 2004.
(28) Boultif, A.; Louër, D. *J. Appl. Crystallogr.* **2004**, *37*, 724−731.
(29) Brese, N.; O'Keeffe, M. *Acta. Crystallogr., Sect. B* **1991**, *47*, 192−197.
(30) Brown, I.; Altermatt, D. *Acta. Crystallogr., Sect. B* **1985**, *41*, 244−247.
(31) Hu, S.-Z.; Xie, Z.-X.; Palenik, G. J. *Acta Phys.-Chim. Sin.* **2012**, *28*, 19.
(32) Favre-Nicolin, V.; Cerny, R. *J. Appl. Crystallogr.* **2002**, *35*, 734−743.
(33) Lämsä, M.; Suorsa, T.; Pursiainen, J.; Huuskonen, J.; Rissanen, K. *Chem. Commun.* **1996**, *12*, 1443−1444.
(34) Dove, M. T.; Tucker, M. G.; Keen, D. A. *Eur. J. Mineral.* **2002**, *14*, 331−348.
(35) King, G.; Abakumov, A. M.; Woodward, P. M.; Llobet, A.; Tsirlin, A. A.; Batuk, D.; Antipov, E. V. *Inorg. Chem.* **2011**, *50*, 7792−7801.
(36) Hamilton, W. C. *Acta Crystallogr.* **1965**, *18*, 502−510.
(37) Li, Y.; Zheng, G.; Lin, C.; Lin, J. *Solid State Sci.* **2007**, *9*, 855−861.
(38) She, Y.-J.; Zhao, S.-P.; Tian, Z.-F.; Ren, X.-M. *Inorg. Chem. Commun.* **2014**, *46*, 29−32.
(39) Lee, B.; Stoumpos, C. C.; Zhou, N.; Hao, F.; Malliakas, C. D.; Yeh, C.-Y.; Marks, T. J.; Kanatzidis, M. G.; Chang, R. P. *J. Am. Chem. Soc.* **2014**, *136*, 15379−15385.
(40) Kitaigorodskii, A.; Struchkov, Y.; Khotsyanova, T.; Vol'pin, M.; Kursanov, D. *Bull. Acad. Sci. USSR* **1960**, *9*, 32−36.
(41) Wang, J.; Toby, B. H.; Lee, P. L.; Ribaud, L.; Antao, S. M.; Kurtz, C.; Ramanathan, M.; Von Dreele, R. B.; Beno, M. A. *Rev. Sci. Instrum.* **2008**, *79*, No. 085105.
(42) Larson, A. C.; Von Dreele, R. B. General Structure Analysis System. LANSCE, MS-H805, Los Alamos, NM, 1994.
(43) Juhas, P.; Davis, T.; Farrow, C. L.; Billinge, S. J. *J. Appl. Crystallogr.* **2013**, *46*, 560−566.
(44) Farrow, C.; Juhas, P.; Liu, J.; Bryndin, D.; Božin, E.; Bloch, J.; Proffen, T.; Billinge, S. *J. Phys.: Condens. Matter* **2007**, *19*, 335219.
(45) Momma, K.; Izumi, F. *J. Appl. Crystallogr.* **2011**, *44*, 1272−1276.
(46) Kresse, G.; Furthmüller, J. *Phys. Rev. B* **1996**, *54*, 11169.
(47) Kresse, G.; Hafner, J. *J. Phys.: Condens. Matter* **1994**, *6*, 8245.
(48) Perdew, J. P.; Burke, K.; Ernzerhof, M. *Phys. Rev. Lett.* **1996**, *77*, 3865.